Hydrodynamic Characteristics of a Small Bee in Hovering Flight

Ki-Deok Ro[†] · Kwang-Seok Kim*

Abstract : The three-dimensional flows in the Weis-Fogh mechanism are studied by flow visualization and numerical simulation by the vortex method. The vortex method, especially the vortex stick method, is employed to investigate the vortex structure in the wake of the two wings. The pressure is estimated by the Bernoulli equation, and the lift on the wing are also obtained. As the results the eddies near the leading edge of each wing in the fling stage take a convex shape because the eddies shed from both tips entrain the flows and the downwash in the rotating stage is deflected toward the outside because the outside tip vortex is stronger than the inside one. And the lift coefficient on the wings in this mechanism is almost independent of the Reynolds number.

Key words : Computational Fluid Dynamics, Vortex Method, Unsteady flow, Random Walk Method

1. Introduction

The Weis-Fogh mechanism, discovered by analyzing the wing motion in the hovering fight of a small insect called Encarsia formosa, is an efficient mechanism of lift generation[1].

The motion of the wings in the Weis-Fogh mechanism as shown in Fig. 1 may consist of five stages.

Figure 1(a) is the "Clap"stage, in which the two wings close touching their leading edges. Figure 1(b) is the "Fling" stage, in which the two wings open touching their trailing edges. Figure 1(c) is the "Rotating" stage, in which the two wings rotate in
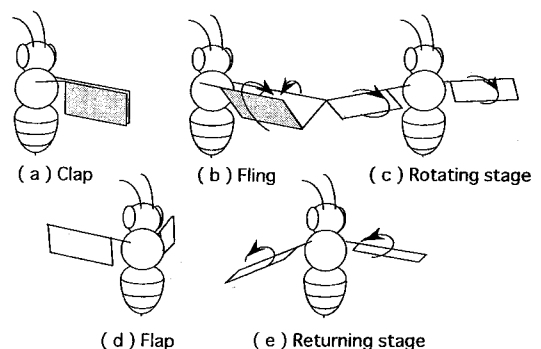

(a) Clap   (b) Fling   (c) Rotating stage

(d) Flap   (e) Returning stage

Fig. 1 Motion of the wing in the Weis-Fogh mechanism

† Corresponding Author(School of Mechanical and Aerospace Engineering · Institute of Marine Industry, Gyeongsang National University), E-mail:rokid@gaechuk.gsnu.ac.kr, Tel: 055)640-3123
* Graduate school of Gyeongsang National University, Department of Mechanical system Engineering

the horizontal plane with the center corresponding to the insect's body. Figure 1(d) is the "Flap"stage, in which the wings change the angle of attack, and Figure 1(e) is the "Returning"stage, in which the wings return to the position of the "Clap"stage. These stages are repeated and the lift on each wing is always generated in the upward direction. In this figure, the insect is on the hovering fight and the arrows indicate the direction of circulation around wings. Lighthill[2] has studied the two-dimensional flow in this mechanism by the potential theory. Maxworthy[3], through the two-dimensional modeling experiment of this mechanism, had visualized the circulation which happened around the wing at the stage of Fling, also sketching the vortex around the wing as for the three-dimensional flow. However, there had not been any theoretical study on the three-dimensional flow of Weis-Fogh mechanism, also the visualization experiment being ended up only at the stage of Fling. Hence, in this study, it was aimed to clearly understand the three-dimensional flow around the wing at the fling and the following rotating stages, by way of the visualization experiment and the numerical calculation utilizing the discrete vortex method. The flow around the wing, as anticipated in Fig. 1, was fully three-dimensional and unsteady. As the movement of wing is also complicated, the finite element method as well as the finite-difference method, which must construct meshes in every time step, are not suitable for this kind of simulation. Therefore, in this numerical calculation, the discrete vortex method[4],[5], which did not need the application of mesh and was useful for

the separation flow, was decided to be introduced. Also, in this calculation, the viscous diffusion of the fluid was expressed by Random walk method[6].

2. Flow Visualization

2.1 Experimental method

The flow patterns around the wings were visualized by titanium tetrachloride, which generates a thick mist of HCI. The apparatus for the experiments was as follows. The wings were made of acryl and each had a square shape with a 70-mm chord length, a 140-mm span, and a 2-mm thickness.

The two wings were set to move symmetrically, and the motion was controlled by hand. The rods to control the wings' motion were connected to wings at their trailing edges as shown in Fig. 2, unlike Maxworthy's experiments[3], in which they were connected with the wings at their leading edges.
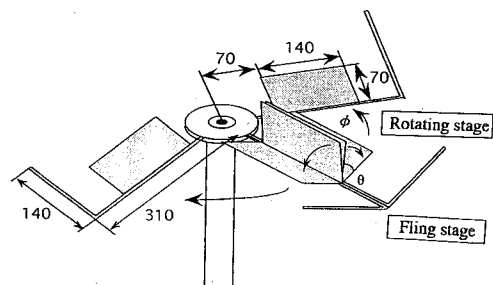

Fig. 2 Schematic diagram of experimental apparatus(unit :mm)

Therefore, the wings were rotated about their trailing edges in the fling stage, and they translated (or rotated) with their trailing edges leading. The edges and the tips of the wings were coated with
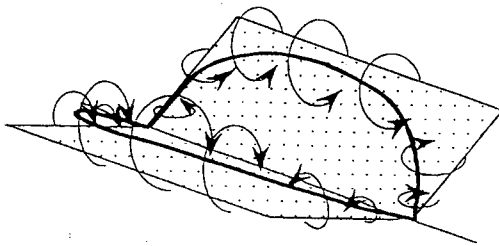
TiCl4just before the wings opened. The flow patterns were recorded by a video camera.

2.2 Experimental results and discussion

The flow patterns in the fling stage only are shown in Fig. 3, in which (a) is the photograph of a flow visualization and (b) is a sketch of the structure of vortices under the same condition as is (a).
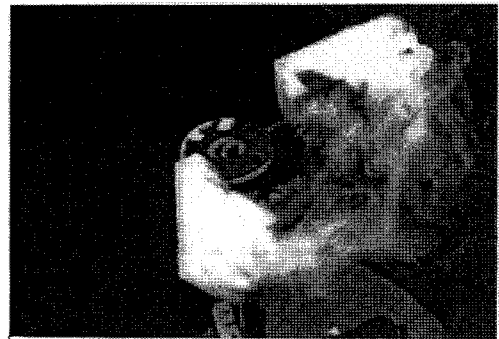

(a) Photograph

(b) Sketch of vortex structure

Fig. 3 Visualization of flowfield around the wings in the fling stage ($Re = 400, \theta = \pi/3$)

The Reynolds number is defined by $Re = \Omega c^2 / \nu$, where Ω is the angular velocity of rotation in the fling, c is the chord length, and ν is the kinematic viscosity. In this figure, the eddies formed by the shearing layers shed from the leading edges are located near the leading edges. These eddies are known to increase the lift in the fling stage. The eddies near

the leading edge of each wing take a convex shape because the eddies shed from both tips of the wings entrain the flows.

The flow pattern in the rotating stage, as shown in Fig. 4, becomes complicated owing to the interaction among the eddies from the leading edges and the tips.

(a) Photograph
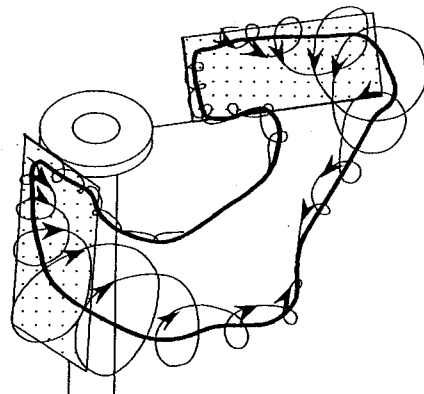
(b) Sketch of vortex structure

Fig. 4 Visualization of flowfield around the wings in the rotating stage (Re=400, $\theta = \pi/3, \phi = \pi/3$)

The strongest eddies are those from the leading edges, and the eddy from one wing is connected to the one from the other wing. The flow is formed by three-dimensional vortices, and a sketch is presented in Fig. 4(b).

3. Numerical Study

3.1 Method of simulation

In this study, the so-called vortex stick method was employed, in which all the vortex filaments are divided into several cylindrical vortex sticks[7] as expressed in figure 5

In the figure, the i-th vortex stick was defined with the 8quantities such as $r_i(x, y, z)$, the position of the center, $\omega_i(\omega_x, \omega_y, \omega_z)$, the vector of vorticity, σ_i, the radius of vortex core and δl_i, the length, while the change of each element with respect to the time was obtained as in the following order.
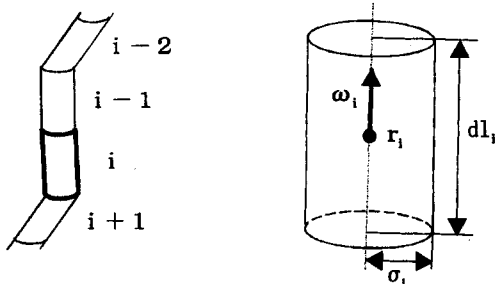

Fig. 5 Vortex filament approximated by vortex stick

Firstly, u_{ij}, the induced velocity at the central position of the i-th vortex stick, was obtained by Biot-Savart's Law as follows.

$$u_{ij} = \frac{1}{4\pi} \int \frac{\omega_i \times (r_i - r_j)}{|r_i - r_j|^3} dr \qquad (1)$$

$r_i{}^t$, the central position of the i-th vortex stick, was moved in every time step Δt by

$$r_i^{t+\Delta t} = r_i^t + u_i^t \Delta t = r_i^t + \sum_{j=1}^n u_{ij}^t \Delta t \qquad (2)$$

Also, the time variation of the vorticity ω_i was calculated from the vorticity transport equation which omitted the viscous term as follows.

$$\frac{D\omega_i^{t+\Delta t}}{Dt} = \omega_i^t \cdot \nabla u_i^t = \omega_i^t \nabla \left(\sum_{j=1}^n u_{ij}^t \right) \qquad (3)$$

In the meanwhile, the time variations of σ_i, the radius of vortex core, and δl_i, the length were obtained from the theorem of Kelvin and from the continuity equation respectively as follows.

$$|\omega_i^{t+\Delta t}| \pi (\sigma_i^{t+\Delta t})^2 = |\omega_i^t| \pi (\sigma_i^t)^2 \qquad (4)$$

$$\pi (\sigma_i^{t+\Delta t})^2 \delta l_i^{t+\Delta t} = \pi (\sigma_i^t)^2 \delta l_i^t \qquad (5)$$

The stretching effect of a vortex filament was represented by the movements of two ends of a vortex stick in the previous study[8], however it was represented by the theorem of Kelvin and the continuity equation, as shown (4) and (5) equations in this study.

From the above equations (2), (3), (4) and (5), the time variations of 8 quantities of vortex stick were able to be obtained, while the viscous diffusion term was approximated by Random walk method. Namely, the displacement vector was obtained from the regular random number with the average value of 0 (zero) and the dispersion of $2\nu\Delta t$ (ν:kinematic viscosity), being added to the right side of equation (2).

The motions of the two wings are completely symmetrical, so that only one wing was considered, and the entire flowfield was obtained by the assumption of symmetry as shown in Fig. 6.
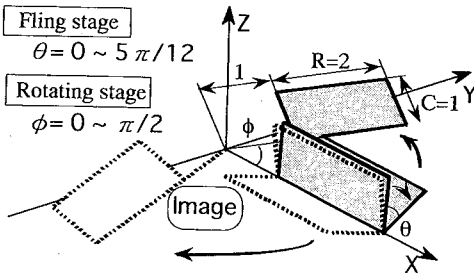
Fig. 6 Three-dimensional analytical model

Each wing was represented by 10 × 20 square panels. Each panel has a ring-type line vortex, represented by the wavy lines in Fig. 7, and then is finally replaced with vortex sticks as shown in Fig. 7.
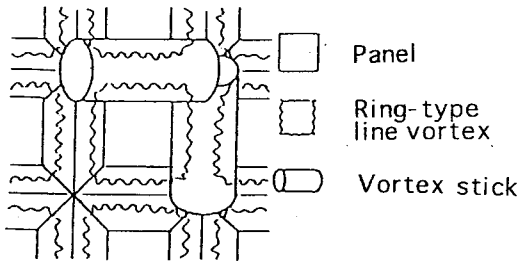

Fig. 7 An enlarged diagram of panel

The circulation of each vortex stick is evaluated by the difference between the circulations of two ring-type vortices that the vortex stick contains. The middle in span direction and a quarter in chord direction of each panel was taken as the control point at which the boundary condition was applied. The boundary condition for determining the circulations of the ring-type vortices was that the normal components of the velocities of the fluid and those of the wing at the control points coincide with each other.

The vortex sticks at the edges and tips of the wing are shed into the flow in each

time step, maintaining their circulations. The structure of the vortices in the flowfield is also ring-like as shown. All the vortex lines are connected and no vortices disappear.

If the vorticity of the ring-type line vortices on the surface of the wing is assumed to be concentrated on the cores, the flow on the surface, excluding the cores, can be considered as potential flow. Therefore, the pressure distribution on the wing can be evaluated by the Bernoulli equation for unsteady flows

$$\frac{\partial \phi}{\partial t} + \frac{u^2}{2} + \frac{p}{\rho} = \text{constant} \qquad (6)$$

where ϕ is the velocity potential, u is the local velocity, p is the pressure, and ρ is the density of the fluid. For calculating the forces on the wing, only the forces due to the pressure are considered.

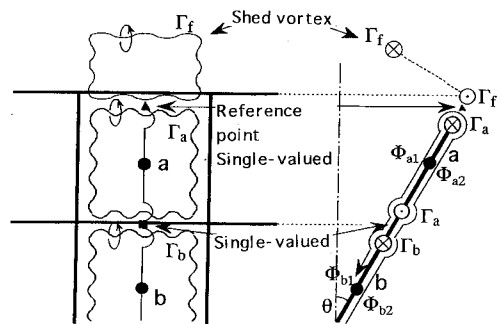The calculation method for the force on the wing is shown in Fig. 8.

Fig. 8 The calculating method for force on the wing

The wing is approximated as a flat plate without thickness, so that only the difference between the pressures on both sides of the wing should be considered.

Only the first term in Eq.(6) is different, that is, this term is multi-valued, but the other terms are not different between the two sides, and those are single-valued. Therefore, the first term will be evaluated here. For example, since the difference of the velocity potential between both sides of the 'a' point in Fig. 8, which is $(\Phi_{a1} - \Phi_{a2})$, corresponds to the circulation Γ_a of the ring-type line vortex, the first term of Eq.(6) on that point can be obtained by estimating the variation of the circulation with time.

$$\frac{\Phi_{a1}}{\partial t} - \frac{\Phi_{a2}}{\partial t} = \frac{\Gamma_a^t - \Gamma_a^{t-\triangle t}}{\triangle t} = \dot{\Gamma}_a \qquad (7)$$

As the same procedure , that on the 'b' point is expressed as

$$\frac{\Phi_{b1}}{\partial t} - \frac{\Phi_{b2}}{\partial t} = \frac{\Gamma_b^t - \Gamma_b^{t-\wedge t}}{\triangle t} = \dot{\Gamma}_b \qquad (8)$$

The force on the perpendicular direction to the surface of the wing F is calculated by

$$F = \int p ds = -\rho \sum_{j=i}^{n} \dot{\Gamma}_j \triangle S_j \qquad (9)$$

where the term $\dot{\Gamma}_j$ represents the time-variations of the circulations in the j-th panel, which is evaluated as shown in Eq.(7) and $\triangle S_j$ is the area of the panel. All the Γ_j on the surface affect the force and they are ring-type. Therefore, the force remains the same whether it is calculated the spanwise or chordwise. The lift, which is the z-direction component of the force in Fig. 6, is expressed as

$$L = -\rho (\sum_{j=1}^{n} \dot{\Gamma}_j \triangle S_j) \sin \theta \qquad (10)$$

where θ is the opening angle shown in Fig. 6.

3.2 Numerical results and discussion

For easy comparison with the experimental results, the calculating conditions were made similar to the experimental conditions. The chord length c and the span R of the wing are 1.0 and 2.0 respectively; the time step $\triangle t$ is 0.05; the angular velocity Ω is 1.0 both in the fling and rotating stages; and the distance form the z-axis to the middle of the wing span is 2.0. The results are represented as a function of the Reynolds number Re, the opening angle θ, and the rotating angle ϕ.

The flow patterns for various Reynolds numbers in the fling stage are shown in Fig. 9.
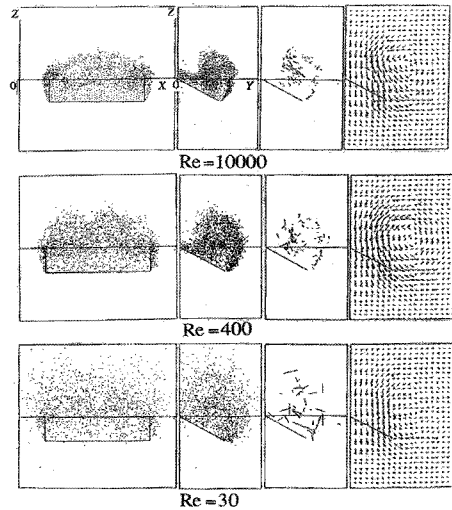

Fig. 9 Flowfield around the wing in the fling stage $(\theta = 2\pi/3)$

The figures in the first and second columns represent the distributions of the

vortex sticks in the z-x and z-y planes respectively; and the third and last columns show the stick traces and the velocity fields in the z-y plane in the cross section at the middle of the wing span, respectively. The distributions of the vortex sticks and the stick traces are scattered more at low Reynolds numbers. This explains the effect of the viscous diffusion. In the first column, the distribution of the vortex sticks is convex in structure, and this corresponds to the results obtained by flow visualization. The velocity fields show that a large circulation in the opposite direction to the opening is formed behind the leading edge of the wing.

The flow patterns for various opening angles in the fling stage are shown in Fig. 10.

A large structure of the vortex shed from the leading edge is located near the leading edge as seen from the distribution of vortex sticks, and this agrees well with the results of flow visualization shown in Fig. 3. The stick traces show that flow separates from the leading edge and reattaches to the wing with time.
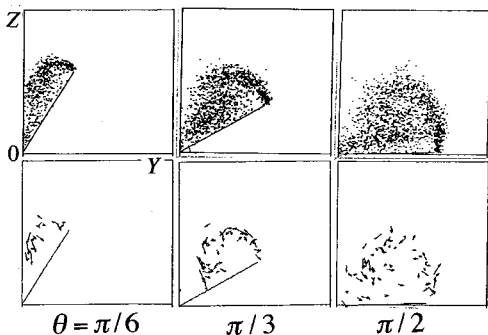

Fig. 10 Vortex sticks and stick traces around the wing in the fling stage ($Re = 400$)

The lift coefficient $C_L = L/(1/2\rho\Omega^2c^2S)$ in the fling stage is shown in Fig. 11 as a function of the opening angle.
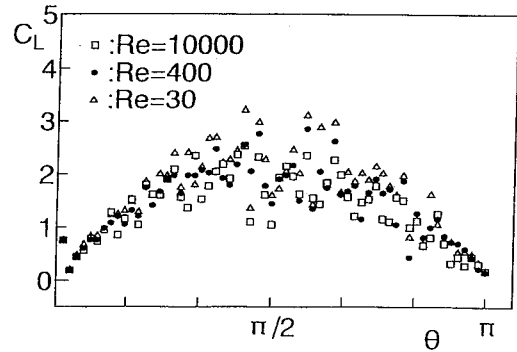

Fig. 11 Lift coefficient in the fling stage

The large fluctuations of the lift coefficients in the Fig. 11 are because the unsteady force of the flow is acted very sensitively on the wing, for the wing is approximated as a flat plate without thickness in the calculation.

The maximum of the lift, regardless of the Reynolds number, occurs at an opening angle of about $\pi/2$. It is difficult to compare exactly these results with the experimental results by Spedding and Maxworthy[9] because the angular velocity in their experiments changes with time. But the calculation results agree qualitatively with the experimental results because the lift is maximum at an opening angle of $\theta = \pi/2$ and minimum at $\theta = 0$ and $\theta = \pi$.

The flow patterns for various rotating angles are shown in Fig. 12.

In this calculation, the wing opens up to $\theta = \pi/3$ and moves to the rotating stage. In this figure P, which is fixed on the wing as shown in Fig. 12, represents an axis of coordinates in the horizontal and

perpendicular plane to the span direction of the wing. As the case was for the rotating stage, the separation happened at the leading and trailing edges of the wing, while the distribution of vortex stick became longer as the wing rotated.
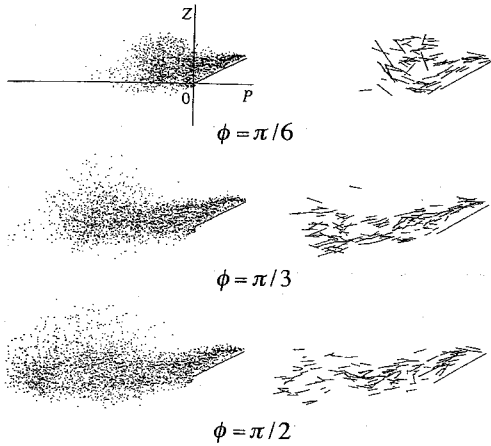

$\phi = \pi/6$

$\phi = \pi/3$

$\phi = \pi/2$

Fig. 12 Vortex sticks and stick traces around the wing in the rotating stage. ($Re = 400,\ \theta = \pi/3$)

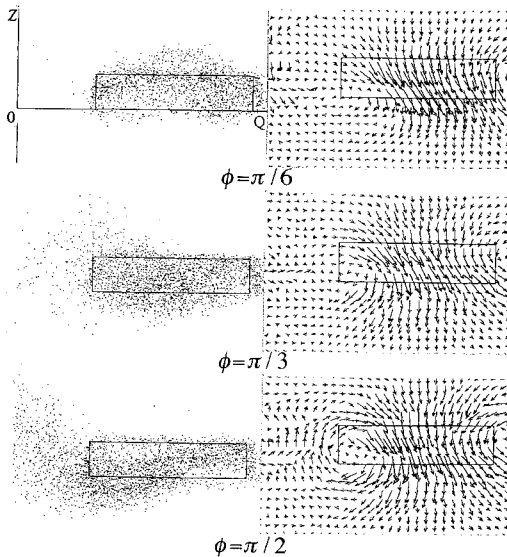$\phi = \pi/6$

$\phi = \pi/3$

$\phi = \pi/2$

Fig. 13 Vortex sticks and velocity vectors around the wing in the rotating stage ($Re = 400, \theta = \pi/3$)

Under the same conditions as in Fig.

12, the flow patterns in the Z–Q plane are shown in Fig. 13.

In this figure Q, which is also fixed on the trailing edge of the wing in the rotating stage, represents the span direction of the wing. The velocity fields in the second column show that the flow near the center of the upper surfer of the wing is accelerated by the tip vortices in the opposite direction. The velocity fields show that the downwash is deflected toward the outside because the outside tip vortex is stronger than the inside one. In the first column, the vortices of the convex type at the rotating angle $\phi = \pi/6$ flow along the trailing edge with an increase of the rotating angle ϕ because of the downwash by tip vortices. In the first columns of Fig. 12 and 13, the vortex sticks are distributed in the direction opposite to the moving direction of the wing. This means that the vortices between the wings are connected to each other and it agrees well with the results of the flow visualization shown in Fig. 4. The lift coefficients for various Reynolds numbers in the fling and rotating stages are shown in Fig. 14.
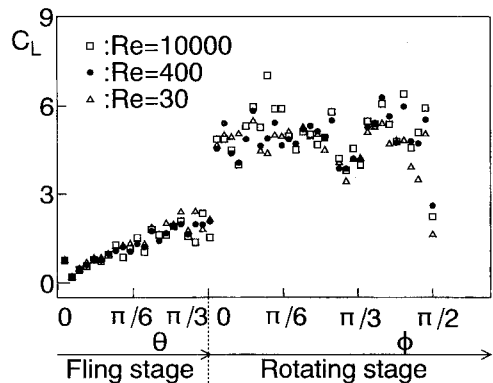

Fig. 14 Lift coefficient in the fling and rotating stages ($\theta = \pi/3$)

This figure shows that the lift coefficient is almost independent of the Reynolds number in the rotating stage as well as in the fling stage. In this study, the angular velocity in the rotating stage Ω is unity as well as that in the fling stage. Therefore, the moving velocity of the edge at the middle of the span in the rotating stage is twice as large as that in the fling stage. If the lift coefficient is nondimensionalized by he middle speed of the wing span in the rotating stage, this coefficient in the rotating stage should be the quarter of the present value.

4. Conclusion

The three-dimensional flows in the Weis-Fogh mechanism were studied by flow visualization and numerical simulation using the vortex method. In this study, the viscosity of the fluid was represented by the random walk method.

(1) The flow patterns around the wings, which are widely different from those in the two-dimensional flow, are strongly influenced by the tip vortices.

(2) The eddies near the leading edge of each wing in the fling stage take a convex shape because the eddies shed from both tips entrain the flows.

(3) The downwash in the rotating stage is deflected toward the outside because the outside tip vortex is stronger than the inside one.

(4) The lift coefficient on the wings in this mechanism is almost independent of the Reynolds number.

(5) The discrete vortex method is very effective for simulating this type of flow.

References

[1] Weis-Fogh,T., "Quick Estimates of Flight Fitness in Hovering Animals, Including Novel Mechanism for Lift Production," Journal of Experimental Biology, Vol.59, pp.169-231, 1973.

[2] Lighthill,M.J., "On the Weis-Figh Mechanism of Lift Generation," Journal of Fluid Mechanics, Vol.60, pp.1-17, 1973.

[3] Maxworthy,T., "Experiments on the Weis- Fogh Mechanism of Life Generation by Insects in Hovering Flight," Journal of Fluid Mechanics, Vol.93,pp.47-63, 1979.

[4] Leonard,A., "Vortex method for Flow Simulation," Journal of Computational Physics. Vol.37, pp289-335, 1980.

[5] Sarpkaya,T., "Computational Methods with Vortices," ASME Journal of fluids Engineering, Vol.111, March, pp5-52, 1989.

[6] Chorin,A.J., "Numerical Study of Slightly Viscous Flow," Journal of Fluid Mechanics, Vol.57,pp.785-796, 1973.

[7] Shirayama, S.,et al., "A Three dimensional Vortex Method", AIAA Paper, 85-1488, pp.14-24, 1985.

[8] Ro, K. D. and Tsutahara. M., "Numerical Analysis of Unsteady Flow in the Weis-Fogh Mechanism by the 3D Discrete Vortex Method with GRAPE3A," Transactions of the ASME, Journal of Fluids Engineering, Vol.119, pp. 96-102, 1997.

[9] Spedding,G.R. and Maxworthy,T., "The Generation of Circulation and Lift in a Rigid Two-Dimensional Fling," Journal

of Fluid Mechanics, Vol.165, pp.247-272, 1986.

Author Profile

Ki-Deok Ro

Date of birth : June 16, 1953.
Pukyong National University, 1973 to 1977, Bachelor of Marine Engineering. Kobe University, 1984 to 1986, Master of Mechanical Engineering. Kobe University, 1986 to 1989, Doctor of Mechanical Engineering. Mobil oil Company, 1977 to 1979, Marine Engineer. National Tongyeong Fisheries College, 1979 to 1995, Professor. Gyeongsang National University, 1995 to present, Professor.

Kwang-seok Kim

Date of birth : Nomember 06, 1980.
Geyongsang National University, 2000 to 2006, Bachelor of Marine Engineering. Graduate School of Gyeongsang National University, 2008 to present, Master course student.